

STUDY OF PHOTOPRODUCTION OF NEUTRAL MESONS USING THE CRYSTAL BARREL AT ELSA

PNPI participants of the CB@ELSA Collaboration:

D.E. Bayadilov, Yu.A. Beloglazov, A.B. Gridnev, I.V. Lopatin, D.V. Novinsky, A.K. Radkov, V.V. Sumachev

1. Introduction

Due to their substructure, nucleons exhibit a rich spectrum of excited states. In spite of considerable theoretical achievements, attempts to model the nucleon spectrum with three constituent quarks and their interactions still fail to reproduce experimental findings in important details. In most quark-model based calculations, more resonances are found than have been observed experimentally. However, the quark model is only an approximation and may overpredict the number of states. Alternatively, these *missing resonances* could as well have escaped experimental observation due to a weak coupling to $N\pi$ which makes them unobservable in elastic πN scattering.

Resonances with small $N\pi$ coupling are predicted to have sizable photocouplings. Thus, the photoproduction of baryon resonances provides an alternative tool to study nucleon states. New facilities at ELSA in Bonn, GRAAL at Grenoble, CLAS at Jefferson Lab, MAMI-C at Mainz, and Spring-8 (Hyogo) offer the possibility to investigate photoproduction for $E_\gamma > 1$ GeV and to study nucleon resonances above the first and second resonance region.

Good angular coverage is needed to be able to extract the resonant and non-resonant contributions. The Crystal Barrel detector at ELSA is thus an ideal tool for studying nucleon resonances.

2. Experimental setup

The experiment was carried out at the electron accelerator ELSA. The maximum available electron energy is 3.2 GeV. The experimental setup is shown in Fig. 1.

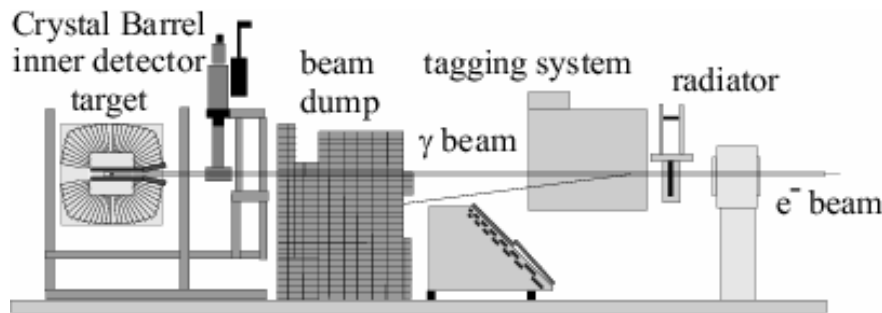


Fig. 1. Experimental setup at ELSA in Bonn

The electrons hit a radiator target, where they produce bremsstrahlung. The energy of photons, in the range between 25% and 85% of the primary electron energy, was determined *via* the detection of the corresponding scattered electrons in the tagging system (“tagger”) consisting of a dipole bending magnet and two detecting parts – an array of fourteen scintillation counters to provide fast timing information and two multiwire proportional chambers (MWPCs) with a total of 348 channel to provide information about trajectories of the scattered electrons. Each scintillator of the array was read out *via* two photomultiplier tubes attached from both sides. A logical OR of the left-right coincidence from all scintillators was required in the first-level trigger.

The tagger was calibrated by direct injection of a very low intensity e^- -beam of 600 or 800 MeV, after removing the radiator. Variation of the magnetic field of the tagging dipole magnet enabled a scan of several spatial positions over MWPCs. For a given wire, the electron momentum is proportional to the magnetic

field strength. The calibration was checked [1] by a Monte Carlo simulation of electron trajectories through the tagger. Geometry of the setup, dimensions of the electron beam, angular divergences, multiple and Møller scattering in the radiator foil and air were taken into account. From these simulations, the energy corresponding to each MWPC wire was obtained by a polynomial fit. The uncertainty of the simulation was estimated to be of the same order of magnitude as the “energy width” of the respective wire.

The Crystal Barrel forms the central component of the experiment. It consists of 1380 CsI(Tl) crystals with a length of 30 cm ($16 X_0$) and has an excellent photon-detection efficiency. The large solid-angle coverage (the 12° opening on either side of the barrel is necessary for technical reasons) and the high granularity allow for reconstruction of multi-photon final states. The spatial resolution determined by the size of individual crystal is at a level of 20 mrad ($\approx 1.1^\circ$); it allows the separation of two photons stemming from the decay of π^0 meson with a maximum momentum 1 GeV/c corresponding to a minimum opening angle of 16.6° . The energy resolution of the calorimeter is empirically described by $\sigma_E/E = 2.5\%/[E(\text{GeV})]^{0.25}$.

The three-layer scintillating fiber detector was inserted into the inner cavity of the Crystal Barrel to identify charged particles leaving the target and to determine their intersection point with the detector. The fibres are 2 mm in diameter; one of the layers was straight, the fibers of other two layers encircled the target with $\pm 25^\circ$ with respect to the first layer. The innermost layer corresponds to a solid angle of 92.6% of 4π .

The coincidence between tagger and scifi detector provided the first-level trigger of the experiment. From the hit pattern in the Crystal Barrel, a fast cluster logic determined the number of “particles” defined by clusters of contiguous crystals with individual energy deposits above 15 MeV. A second-level trigger was generated for events with two or more particles in the cluster logic. In the data analysis, clusters with two local maxima were split into two particles sharing the total energy deposit. The offline threshold for accepted particles was set to 20 MeV. The proton kinetic energy had to exceed 35 MeV to traverse the inner two scifi layers and to produce a trigger. A proton of 90 MeV was needed to reach the barrel calorimeter and to deposit the minimum cluster energy of 20 MeV.

The Crystal Barrel acceptance was determined from the Monte Carlo simulation. It vanishes for forward protons leaving the Crystal Barrel through the forward hole and for protons with very low energies.

3. The reaction $\gamma p \rightarrow p\pi^0$

Differential cross sections of the π^0 photoproduction were determined [2, 3] in two run periods with different primary electron energies of 1.4 and 3.2 GeV providing a total range of photon energies from 0.3 to 3 GeV. The π^0 mesons were reconstructed from their $\pi^0 \rightarrow \gamma\gamma$ decays. The compatibility of events with the hypothesis $\gamma p \rightarrow p\gamma\gamma$ was tested in a one-constraint kinematical fit imposing energy and momentum conservation but leaving the proton 3-momentum as adjustable quantity. Figure 2 shows the $\gamma\gamma$ invariant mass spectrum after a 10^{-4} confidence level cut in the 1C kinematical fit. The π^0 -meson and η -meson signals are observed above a small residual background. There are 2.6×10^6 events due to $\gamma p \rightarrow p\pi^0$.

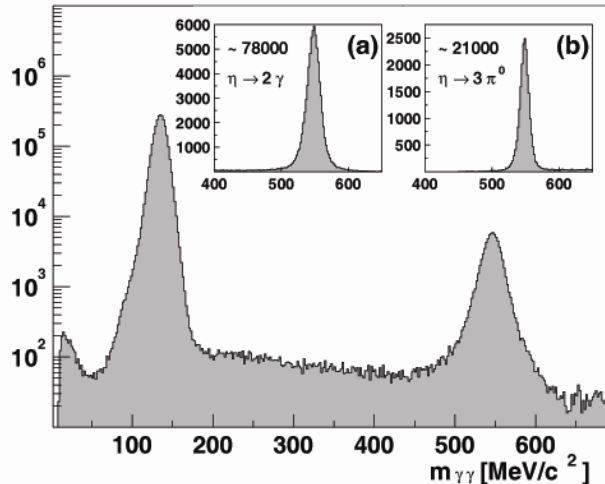


Fig. 2. Spectra of invariant $\gamma\gamma$ masses. Inserted in the top are spectra for the two different modes of the η decay

The differential cross sections can be calculated from the number of data events identified in the respective E_γ channel using the relation

$$\frac{d\sigma}{d\Omega} = \frac{N_{\pi^0 \rightarrow 2\gamma}}{A_{\pi^0 \rightarrow 2\gamma}} \cdot \frac{1}{N_\gamma N_p} \cdot \frac{1}{\Delta\Omega} \cdot \frac{\Gamma_{total}}{\Gamma_{\pi^0 \rightarrow 2\gamma}}, \quad (1)$$

where the quantities are:

- $N_{\pi^0 \rightarrow 2\gamma}$ – the number of events in $(E_\gamma, \cos\theta_{cm})$ bin;
- $A_{\pi^0 \rightarrow 2\gamma}$ – the angular acceptance in $(E_\gamma, \cos\theta_{cm})$ bin;
- N_γ – the number of primary photons in E_γ bin;
- N_p – the number of protons in the target (in $1/\text{cm}^2$);
- $\Delta\Omega$ – the solid-angle interval;
- $\frac{\Gamma_{\pi^0 \rightarrow 2\gamma}}{\Gamma_{total}}$ – the decay branching ratio.

The solid-angle interval is $\Delta\Omega = 2\pi \cdot \Delta(\cos\theta_{cm})$ where $\Delta(\cos\theta_{cm}) = 0.1$ gives the bin width of the angular distributions, subdividing $\cos\theta_{cm}$ into 20 bins. Photon-energy bins of 25 MeV were chosen for the 1.4-GeV data set. The 3.2-GeV data are presented in bins of about 50 MeV, 100 MeV and 200 MeV in the intervals $E_\gamma \in [750, 2300]$, $[2300, 2600]$, $[2600, 3000]$, respectively. In total, approximately 1500 experimental points were obtained.

From the differential cross sections, the total cross section was determined by integration. The integration was performed by summing over the differential cross sections and using extrapolated values from the fit for angular bins with no data. In the total cross section, shown in Fig. 3, clear peaks are observed for the first, second, and third resonance regions. The fourth resonance region exhibits a broad enhancement at W about 1900 MeV. The decomposition of the peaks into partial waves was based on a coupled-channel partial-wave analysis (PWA) in the framework of an isobar model. Resonances are described by Breit-Wigner amplitudes, except for strongly overlapping states which are described in K -matrix formalism. In total, the masses, widths, helicity ratios, and contributions to the cross section for π^0 photoproduction were determined for twelve N -resonances and for seven Δ -resonances as a result of such analysis.

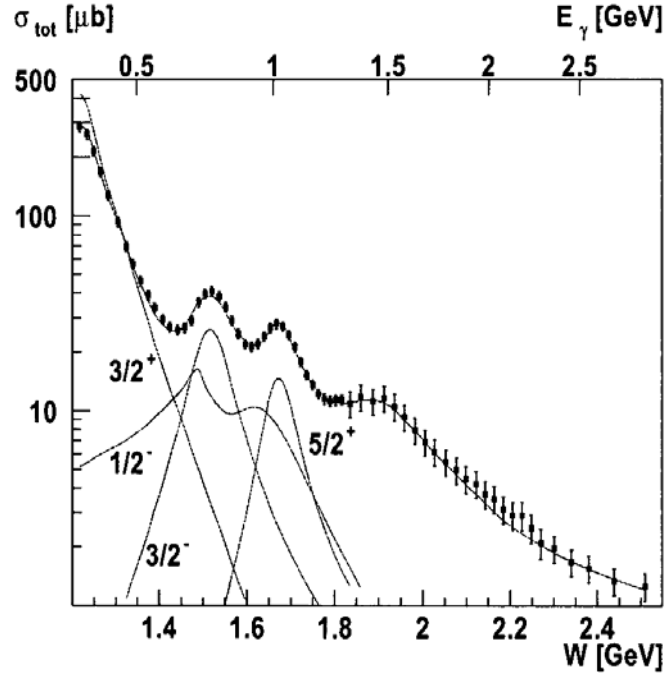


Fig. 3. Total cross section (logarithmic scale) for the reaction $\gamma p \rightarrow p\pi^0$ obtained by integration of angular distributions of the CB-ELSA data. The solid line represents the results of the PWA. Four individual contributions to the cross section are also shown

4. The reaction $\gamma p \rightarrow p\eta$

Differential cross sections of η photoproduction were determined [4, 5] in the run with primary electron energy of 3.2 GeV providing a total range of photon energies from the threshold (0.75 GeV) to 3 GeV. The η meson was reconstructed from two different modes of its decay: $\eta \rightarrow 2\gamma$ with $BR = (39.4 \pm 0.3)\%$ and $\eta \rightarrow 3\pi^0 \rightarrow 6\gamma$ with $BR = (32.5 \pm 0.3)\%$. The 2γ invariant mass spectrum from events with two photons detected (after a kinematical fit to $\gamma p \rightarrow p\gamma\gamma$) and the $3\pi^0$ invariant mass distribution for events with six photons detected (after a kinematical fit to $\gamma p \rightarrow p3\pi^0$) are shown in the top part of Fig. 2. In both cases the η meson is observed above a small background which was subtracted in further processing.

The angular bin was chosen to be equal $\Delta(\cos\theta_{\text{cm}}) = 0.1$, photon-energy bins varied from 50 MeV at the lowest E_γ to 200 MeV at highest E_γ . The ratio $\eta \rightarrow 3\pi^0$ to $\eta \rightarrow 2\gamma$ was determined for each bin and histogrammed, giving $\Gamma_{\eta \rightarrow 3\pi^0} / \Gamma_{\eta \rightarrow 2\gamma} = 0.822 \pm 0.002_{\text{stat}} \pm 0.004_{\text{syst}}$. This value agrees well the Particle Data Group value and demonstrates the good understanding of the detector response. It is thus justified to add the data from the two channels $\eta \rightarrow 2\gamma$ and $\eta \rightarrow 3\pi^0 \rightarrow 6\gamma$. In total, approximately 700 experimental points were obtained.

The total cross section was determined by integrating the differential cross sections. The obtained total cross sections are shown in Fig. 4 vs photon energies in comparison with the results of earlier experiments. The new CB-ELSA data extends the covered angular and energy range significantly compared to previous measurements.

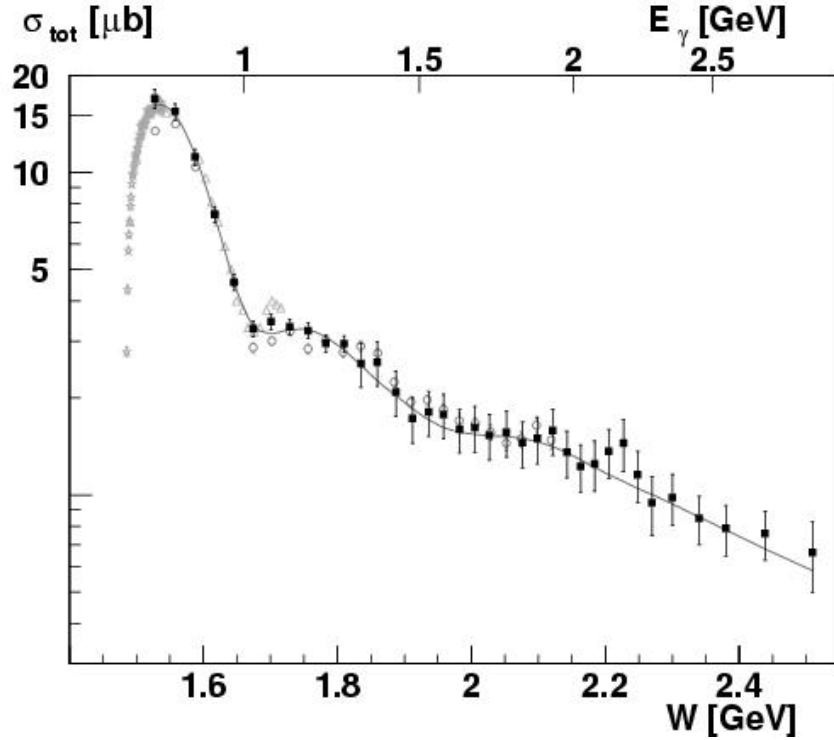


Fig. 4. Total cross section (logarithmic scale) for the reaction $\gamma p \rightarrow p\eta$ obtained by integration of angular distributions of the CB-ELSA data (squares) are shown in comparison with results of earlier experiments

The data obtained are interpreted using a coupled-channel PWA in the framework of an isobar model. This analysis determines parameters (masses, widths, and contributions to the total cross section) of eleven $N\eta$ resonances coupling to $N\eta$. A new state coupling strongly to the η -channel was found, an $D_{15}(2070)$ with a mass of $2068 \pm 22 \text{ MeV}/c^2$ and a width of $295 \pm 40 \text{ MeV}/c^2$. In addition, an indication for a possible new $D_{13}(2200)$ state with a mass of $2214 \pm 28 \text{ MeV}/c^2$ and a width of $360 \pm 55 \text{ MeV}/c^2$ was given also by this analysis. No evidence was found for a third S_{11} resonance for which claims have been reported at masses of $1780 \text{ MeV}/c^2$ and $1846 \text{ MeV}/c^2$.

5. The reaction $\gamma p \rightarrow p\pi^0\pi^0$

At higher energies, multi-meson final states play a role of increasing importance. Above 1900 MeV the spectrum and properties of resonances are rather badly known. Calculations showed that many of these states should have a strong coupling to $\Delta\pi$ and a non-vanishing coupling to γN and hence photoproduction experiments have a good chance to discover such states. Within different $\gamma p \rightarrow N 2\pi$ channels, the $\gamma p \rightarrow p\pi^0\pi^0$ channel is the one best suited to investigate the $\Delta\pi$ decay of baryon resonances. Compared to other isospin channels, many non-resonant “background” amplitudes do not contribute, and this leads to a high sensitivity of the $\gamma p \rightarrow p\pi^0\pi^0$ channel on baryon resonances decaying into $\Delta\pi$.

To investigate the reaction $\gamma p \rightarrow p\pi^0\pi^0$, events with 4 photons are selected [6]. In Fig. 5 the invariant $p\pi^0$ -mass is shown for two \sqrt{s} -bins. At low \sqrt{s} only a peak due to the $\Delta(1232)$ resonance is observed, at higher energies additional structures became visible. In addition to the $\Delta(1232)$, contributions from the $D_{13}(1520)$ and a further state around 1660 MeV are observed. To extract the properties of contributing resonances from the data, a PWA has been performed. Resonances with different quantum numbers were

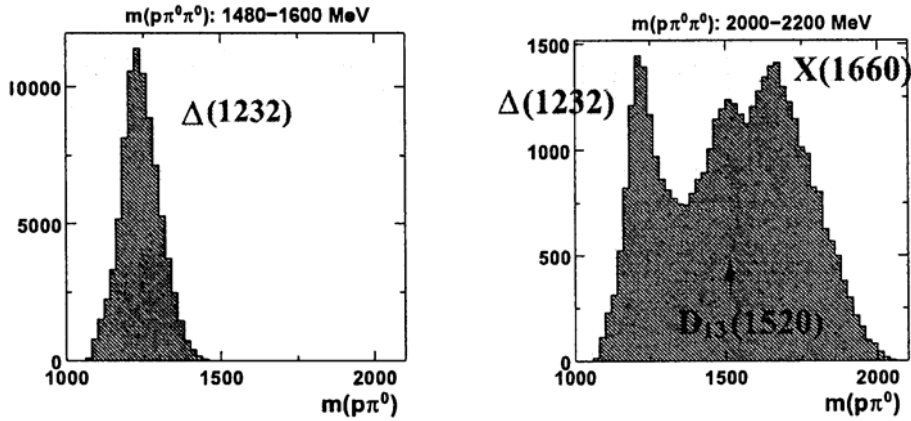


Fig. 5. $p\pi^0$ invariant mass for events with $\sqrt{s} = 1480\text{--}1600$ MeV (left) and $\sqrt{s} = 2000\text{--}2200$ MeV (right)

introduced in different combinations allowing for the following decay modes: $\Delta(1232)\pi$, $N(\pi\pi)_s$, $P_{11}(1440)\pi$, $D_{13}(1520)\pi$ and $X(1660)\pi$. The $\Delta(1232)$ resonance clearly dominates the $p\pi^0$ invariant mass. The PWA attributes most of these events to the $\gamma p \rightarrow D_{13}(1520) \rightarrow \Delta\pi$ amplitude. Another result of the PWA is the observation of baryon cascades.

Shown in Fig. 6 is the total cross section of the reaction $\gamma p \rightarrow p\pi^0\pi^0$ [7] for the two run periods with primary electron energies of 1.4 and 3.2 GeV. For comparison results of earlier measurements are given also. Our data confirms the cross section in the energy range between 700 and 1200 MeV and extends the energy range up to 3 GeV. Deviations are visible between 500 and 700 MeV and at energies above 1200 MeV.

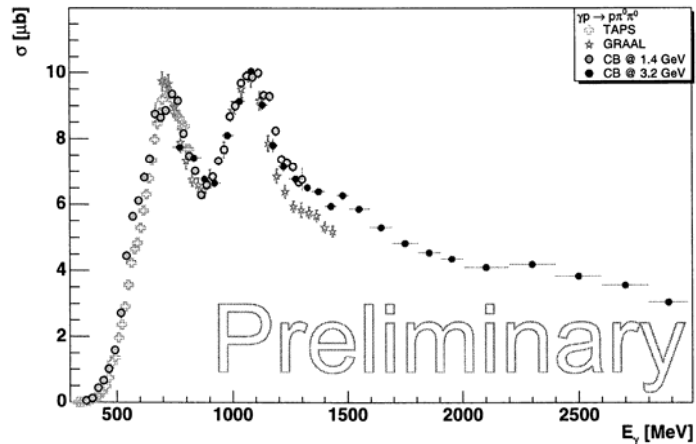


Fig. 6. Total cross section of the reaction $\gamma p \rightarrow p\pi^0\pi^0$ with statistical errors only

6. The reaction $\gamma p \rightarrow p\pi^0\eta$

The reaction $\gamma p \rightarrow p\pi^0\eta$ gives another interesting final state. Here, *e.g.*, the decay of Δ^* resonances into $\Delta\eta$ can be investigated. This decay had the advantage of being isospin selective; no N^* resonances can be produced.

This reaction is well suited to investigate the existence of the negative parity Δ^* -states around 1900 MeV/c². These states would, if they exist, pose a problem for quark model calculations because of their low mass. But so far an evidence for their existence is weak. Only one of the three states, the $D_{35}(1930)$, has 3 stars in the PDG notations. The 1-star $D_{33}(1940)$ resonance can decay with orbital angular momentum zero into $\Delta\eta$, which makes the $p\pi^0\eta$ final state a good place to investigate the existence of this resonance.

With the Crystal Barrel detector at ELSA this final state has been investigated from the threshold up to photon energy of 3 GeV [8]. In Fig. 7 the invariant $p\pi^0$ -masses are shown for three \sqrt{s} -bins. The spectra may be explained by the $\Delta(1232)$ resonance which appears in each \sqrt{s} -bin, indicating possible decay mode *via* $\Delta(1232)\eta$. At two lower \sqrt{s} the $\Delta(1232)\eta$ intermediate state could come from the sequential decay of the

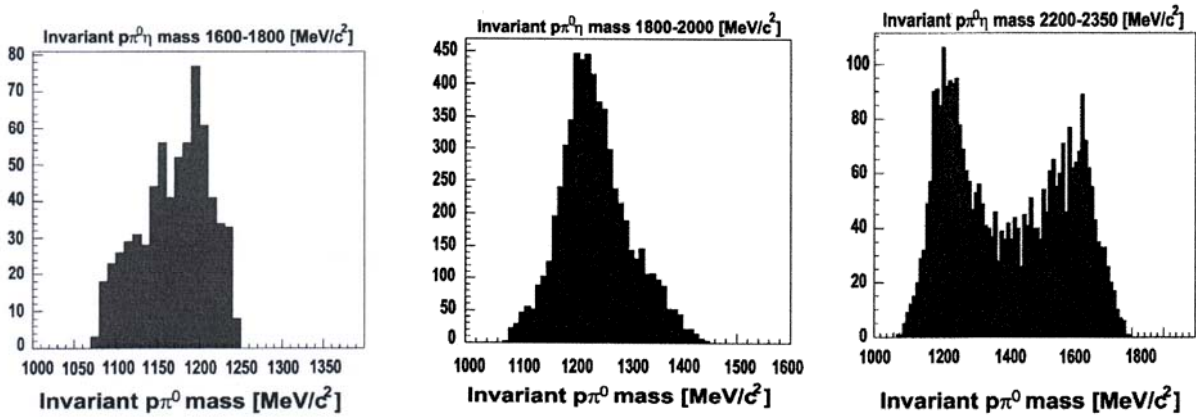


Fig. 7. $p\pi^0$ invariant mass for events with $\sqrt{s} = 1600\text{--}1800$ MeV, $\sqrt{s} = 1800\text{--}2000$ MeV and $\sqrt{s} = 2200\text{--}2300$ MeV

negative parity $D_{33}(1940)$ resonance. In the third case, higher mass contributions at about 1600 MeV/c² become obvious in the $p\pi^0$ subsystem. In addition to the $\Delta(1232)$ resonance there are other interesting structures observed, such as the $a_0(980)$ in the $\pi^0\eta$ invariant mass or the $S_{11}(1535)$ in the Dalitz plot.

To extract the resonance contributions from the data a PWA of the $p\pi^0\eta$ final state has been performed. Three ambiguous solutions were found, which resulted in a similar likelihood being based, at the same time, on quite different sets of contributing amplitudes. All three solutions do need a $D_{33}(\approx 1900)$ state and show indications to baryon cascades

Figure 8 shows the total cross sections of the reactions $\gamma p \rightarrow p\pi^0\pi^0$ and $\gamma p \rightarrow p\pi^0\eta$. Above 2 GeV both cross sections are almost equal in magnitude.

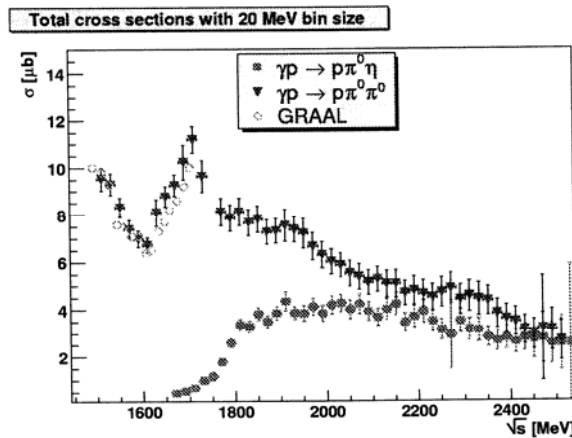


Fig. 8. Total cross sections of the reactions $\gamma p \rightarrow p\pi^0\pi^0$ and $\gamma p \rightarrow p\pi^0\eta$

7. Upgrade of experimental setup

At the next stage of experiments on photoproduction of neutral mesons, measurements of the double polarization parameters of reactions under study are planned. Such kind of measurements provide physicists with a unique information for identification of different baryonic states, especially in the region of overlapping resonances where “missing” baryonic states could be found.

These rather complicated experiments need both a beam of polarized photons and a polarized proton target. To realize this, the upgrade of the experimental setup was performed during 2005–2006. First of all, the Crystal Barrel was moved to another beam-line – Fig. 9. The tagging system installed earlier at this line was modified being equipped with 96 new scintillation counters (with overlapping scintillators of

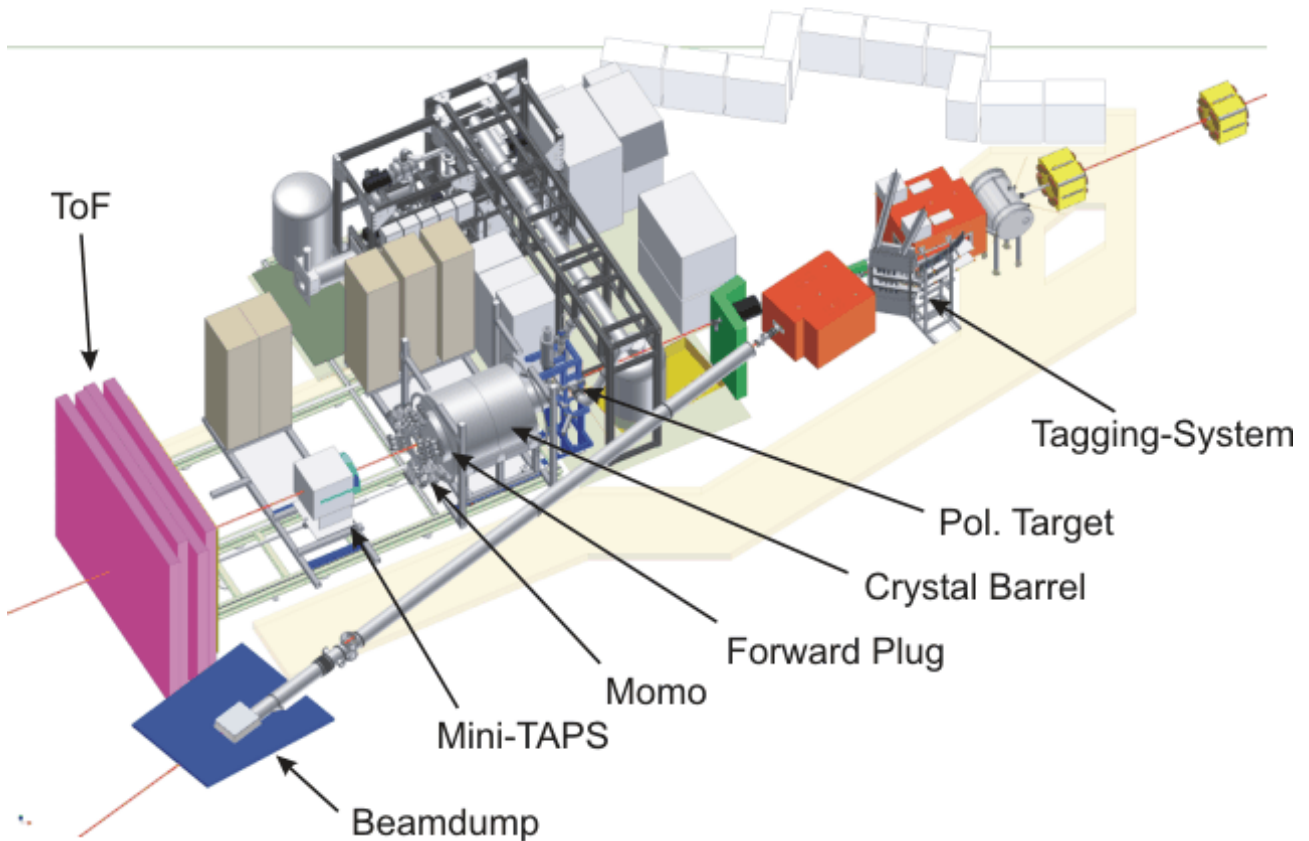


Fig. 9. Disposition of the experimental setup after its upgrading and replacing to another beam-line

varying width) and with an array of 480 scintillating fibres (two layers of 2 mm diameter fibres arranged with overlap). This will allow to tag photons with 18% to 95% of the incoming electron energy with an energy resolution between 0.2% and 2.2%. Linearly polarized photons will be produced by coherent bremsstrahlung at a 100 μm thick diamond crystal, circularly polarized photons – *via* incoherent bremsstrahlung of longitudinally polarized electrons off an amorphous radiator.

Displacement of the Crystal Barrel to another beam-line allowed to insert a longitudinally polarized proton target into the Crystal Barrel inner cavity and to arrange its operation in the “frozen spin” mode by locating a system of polarization “pumping” outside the Crystal Barrel. This system consists of a horizontal dilution refrigerator and a 5 T superconducting polarization magnet, which will be used in the polarization phase together with a microwave system for dynamical nuclear polarization. The polarization will be preserved in the “frozen spin” mode at temperature of about 50 mK by a very thin superconducting solenoid

located within the target cryostat, which will produce a 0.5 T longitudinal holding magnetic field. In general, maximum polarization of 90% is possible. The relaxation time of the target is in the order of 200 hours.

In order to have a possibility to detect photons and charged particles emitted from the target at small angles, the main detector of the setup – the multi-crystal photon spectrometer Crystal Barrel – was equipped in addition with two forward detectors (see Fig. 10) created specially for this purpose. One of them (so called Forward Plug) assembled of 90 CsI(Tl) crystals was inserted into the open forward cone of the Crystal Barrel for registering particles emitted at angles from 10° to 30° and, thus, for increasing the total covered solid angle. 180 overlapping veto-counters made of thin scintillators were placed in front of the CsI(Tl) crystals in order to determine the kind of particle (photon or proton) entering each crystal. Another forward detector (Mini-TAPS) is a “wall” consisting of 216 BaF₂ crystals and 216 veto-counters located in front of crystals; the central crystal was removed to make a hole for the photon beam. The Mini-TAPS registers particles (photons and protons) emitted at angles from 1° to 10°

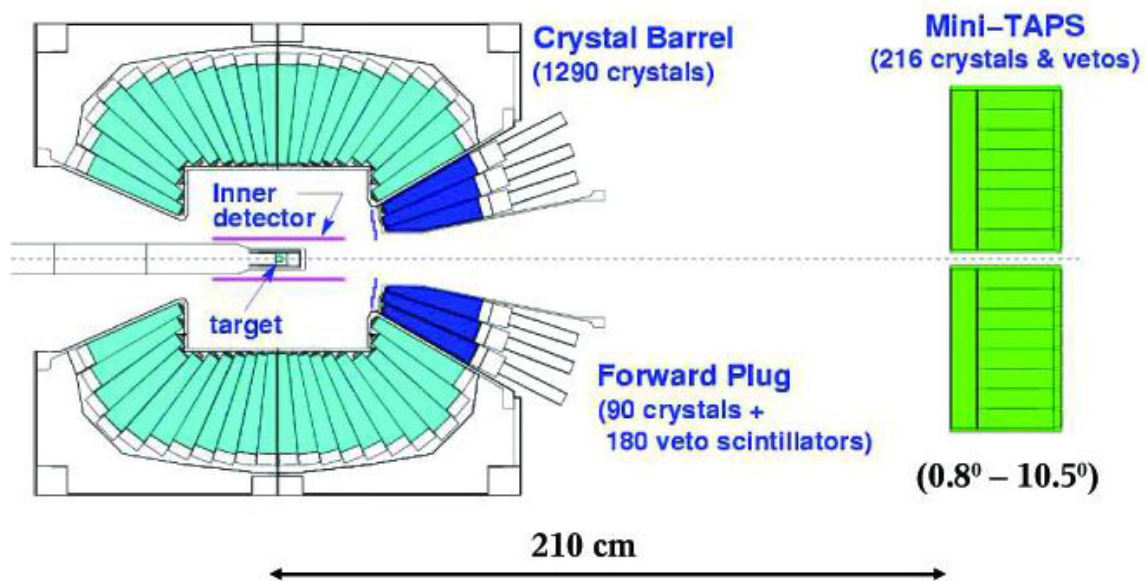


Fig. 10. Schematic drawing (cross section) of two forward detectors

The mostly essential PNPI contribution to the above described upgrade was manufacturing and tuning the system of veto-counters for the Forward Plug. In particular, 180 thin scintillators for these counters were manufactured at PNPI. In Bonn, PNPI physicists participated in assembling the whole system of veto-counters and in tuning the associated electronics.

The new series of experiments with the polarized proton target and polarized photons started in 2007.

References

1. D. Bayadilov *et al.*, Preprint PNPI-2520, Gatchina, 2003. 27 p.
2. O. Bartholomy, ... , Yu. Beloglazov *et al.*, Phys. Rev. Lett. **94**, 012003 (2005).
3. H. van Pee, ... , Yu. Beloglazov *et al.*, Eur. Phys. J. A **31**, 61 (2007).
4. V. Crede, ... , Yu. Beloglazov *et al.*, Phys. Rev. Lett. **94**, 012004 (2005).
5. O. Bartholomy, ... , Yu. Beloglazov *et al.*, Eur. Phys. J. A **33**, 133 (2007).
6. U. Thoma for the CB/ELSA Collaboration, in *Proceedings of the Workshop on the Physics of Excited Nucleons* (Tallahassee, USA, 12 – 15 October 2005), World Scientific Publishing Co., 2006, p. 108.
7. M. Fuchs for the CB/ELSA Collaboration, in *Proceedings of the Workshop on the Physics of Excited Nucleons* (Tallahassee, USA, 12 – 15 October 2005), World Scientific Publishing Co., 2006, p. 324.
8. V. Crede for the CB/ELSA Collaboration, in *Proceedings of the 10th International Conference on Hadron Spectroscopy* (Aschaffenburg, Germany, 31 August – 6 September 2003), AIP Conference Proceedings, **717**, 236 (2004).